SAND2020-1617J

On quantum-dot lasing at gain peak with linewidth enhancement factor $\alpha_H = 0$

Weng W. Chow,[1] Zeyu Zhang,[2] Justin C. Norman,[3] Songtao Liu[2] and John E. Bowers [3]

[1] Sandia National Laboratories, Albuquerque, NM 87185-1086, U.S.A.

[2] Department of Electrical and Computer Engineering, University of California, Santa Barbara, CA 93106 USA.

[3] Institute for Energy Efficiency, University of California, Santa Barbara, CA 93106 USA.

Abstract

This paper describes an investigation of the linewidth enhancement factor α_H in a semiconductor quantum-dot laser. Results are presented on active region parameters and laser configurations important for minimizing α_H. In particular, the feasibility of lasing at gain peak with $\alpha_H = 0$ is explored. The study uses a many-body theory with dephasing effects from carrier scattering treated at the level of quantum-kinetic equations. InAs quantum-dot lasers with different p-modulation doping densities are fabricated and measured to verify calculated criteria on laser cavity design and epitaxial growth conditions.

Quantum well (QW) gain regions have replaced bulk ones for virtually all commercial applications. Further improvement in laser performance may have to come from an underlying physics level. A strong candidate is the class of lasers with quantum-dot (QD) active regions, where quantum confinement increases from one-dimension to three-dimension, or equivalently, electronic density of states reduces from two-dimension (2-d) to zero-dimension (0-d). [1] The atomic (0-d) nature of optical emission was demonstrated in 1990's. [2] [3] Predicted advantages of low lasing threshold, [4] high temperature operation,_[5] tolerance to crystalline defects and optical feedback [6] [7] are being realized.

With successes in threshold performance, attention in QD lasers is shifting towards above-threshold properties. Important for applications, ranging from datacom and telecom to chemical sensing and laser radar, are laser linewidth, [8] chirp during high-speed modulation, [9] [10] and optical feedback sensitivity. [11] A critical gain-medium parameter is the linewidth enhancment factor, [12] [13]

$$\alpha_H = -2K \frac{d(\delta n)}{dN_e} \left(\frac{dG}{dN_e} \right)^{-1}, \tag{1}$$

where δn is the carrier-induced refractive index, G is the intensity gain, N_e is the carrier density and K is the lasing wavevector.

We investigated the minimization of α_H, in particular, feasibility of $\alpha_H = 0$ at the gain peak. This paper describes application of a many-body QD gain theory to identify relevant device parameters and desirable laser configurations. The study involves lasers, each consisting of multiple QWs embedding InAs QDs. The QWs are separated by GaAs barriers and the entire gain region is cladded by graded-index AlGaAs layers. [14] [15] [16] [17] [18] The calculations are for gain and carrier-induced refractive index from one of the QWs, specifically for a 7 nm $In_{0.15}Ga_{0.85}As$ QW with InAs QD density $N_{QD}^{2d} = 5 \times 10^{10}\ cm^{-2}$, and with various p-modulation

doping density and inhomogeneous broadening. These parameters represent tunable criteria in laser cavity design and epitaxial growth conditions for engineering $\alpha_H = 0$ QD lasers.

From semiclassical laser theory, the intensity gain G and carrier-induced refraction index δn at laser frequency ν, are [19] [20]

$$[2K\delta n(\nu) + iG(\nu)]\mathcal{E} = \frac{2\nu}{\varepsilon_0 n_B ch}\left[\sum_n \wp_n \sum_q n_{n,q}^{inh}\, p_{n,q}(\nu) + \frac{1}{A}\sum_k \wp_k p_k(\nu)\right], \quad (2)$$

where c and ε^0 are the vacuum speed of light and permittivity, n_B is the background refractive index, h is the QW width, $\mathcal{E}$ is a weak laser probe field for extracting the susceptibility, A is the QW area, $\wp_n$ and $\wp_k$ are the QD and QW dipole matrix elements. The subscripts n and k label the QD and QW optical transitions, $p_{n,q}$ and p_k are the QD and QW polarizations, and $n_{n,q}^{inh}$ is the density of QDs with electronic structure labeled by q, contributing to the n^{th} QD transition. The computed G and δn are useful in 2 ways. They give the gain parameters at saturated carrier density in the often used class B semiconductor laser model. [21] They are also used in predicting general laser performance (such as light-current characteristics) when the saturated gain and carrier density are clamped at the threshold values. [22]

The calculations start with solving the equations of motion for electron-hole polarizations. For the nth QD transition belonging to the qth population group,

$$\begin{aligned}\frac{dp_{n,q}}{dt} = {} & i\left(\nu - \omega_{n,q}^{(0)}\right)p_{n,q} - i\frac{2\wp_n\mathcal{E}}{\hbar}\left(f_{n,q}^{e} + f_{n,q}^{h} - 1\right) \\ & + \frac{i}{\hbar}\sum_k V_{n,k}\left(f_k^e + f_k^h\right)p_{n,q} + \frac{i}{\hbar}\sum_k V_{n,k}p_k \\ & + S_n^{c-p} + S_n^{c-c}. \end{aligned} \quad (3)$$

In the first line are the the single-particle contributions from frequency detuning and stimulated emission, where $\omega_{n,q}^{(0)}$ is the unrenormalized transition frequency and $f_{n,q}^{\sigma}$ ($\sigma = e$ or h) is the QD

carrier population. The second line contains the many-body corrections due to exchange and excitonic effects, with dependences on the QW carrier population f_k^{σ}. These effects renormalize the transition frequency and light-matter interaction strength via the Coulomb potential energy matrix element $V_{n,k}$. In the third line, S_n^{c-p} and S_n^{c-c} represent the higher-order many-body effects describing dephasing and screening from carrier-phonon and carrier-carrier scattering. The expression for S_n^{c-c} come from continuing the Cluster expansion giving the renormalization contributions to the 2nd level in Coulomb correlations. [23] For S_n^{c-p}, we use a non-perturbative, quantum-kinetic approach adapted from treating carriers and phonons as composite polarons. [24] The corresponding equations of motion for the QW transitions derived similarly, giving,

$$\frac{dp_k}{dt} = i\left(\nu - \omega_k^{(0)}\right)p_k - i\frac{2\wp_k \mathcal{E}}{\hbar}\left(f_k^e + f_k^h - 1\right)$$
$$+\frac{i}{\hbar}\left[A\sum_n V_{n,k}\sum_q n_{n,q}^{inh}\left(f_{n,q}^e + f_{n,q}^h\right) + \sum_{k'} V_{|k-k'|}\left(f_{k'}^e + f_{k'}^h\right)\right] p_k$$
$$+\frac{i}{\hbar}\left[A\sum_n V_{n,k}\sum_q n_{n,q}^{inh} p_{n,q} + \sum_{k'} V_{|k-k'|}p_{k'}\right]$$
$$+S_k^{c-p} + S_k^{c-c}\ , \qquad (4)$$

where $V_{|k-k'|}$ is the QW Coulomb potential matrix element.

Many-body Coulomb effects are important for the QD α_H because they influence the carrier density dependences of shift and broadening of QD resonances. The shift causes semiconductor QDs to deviate from the ideal $\alpha_H = 0$ of an atom. [25] The broadening modifies the shift effects. [20]

Inhomogeneous broadening from QD dimension and composition variations is treated by grouping the QDs according to electronic structure. For the QD density in each group, we assume a Gaussian distribution so that

$$\sum_q n_{n,q}^{inh} \to \int d\omega_n \frac{N_{QD}^{(2d)}}{\sqrt{2\pi}\Delta_{inh}} \exp\left[-\left(\frac{\hbar(\omega_n - \omega_{n,0})}{\sqrt{2}\Delta_{inh}}\right)^2\right], \tag{5}$$

where ω_n is the renormalized frequency of the n^{th} QD transition in the q^{th} group, $\omega_{n,0}$ and Δ_{inh} are the central transition frequency and standard deviation. We assume carrier populations defined by Fermi-Dirac functions, $f_{n,q}^{\sigma} = \{\exp[(\varepsilon_{n,q}^{\sigma} - \mu_{\sigma})/(k_B T)] + 1\}^{-1}$ and $f_k^{\sigma} = \{\exp[(\varepsilon_k^{\sigma} - \mu_{\sigma})/(k_B T)] + 1\}^{-1}$, where $\varepsilon_{n,q}^{\sigma}$ and ε_k^{σ} are the electron and hole ($\sigma = e, h$) energies, k_B is Boltzmann constant and T is the active region temperature. The chemical potential μ_{σ} is determined from the total electron and hole densities, $N_{\sigma} = N_{\sigma'} + \sum_n \sum_q n_{n,q}^{inh} f_{n,q}^{\sigma} + \sum_k f_k^{\sigma}$, where $N_{\sigma'}$ with $\sigma' = d$ or p for $\sigma = e$ or h, respectively, is the doping density.

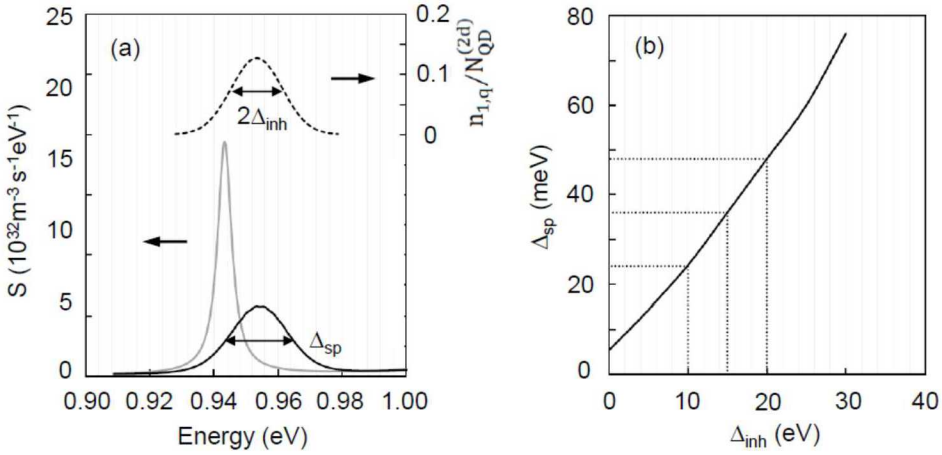

Figure 1. (a) Spontaneous emission spectra for carrier density $N_e = 10^{11}\ cm^{-2}$ and inhomogeneous broadening $\Delta_{inh} = 0$ and $8\ meV$ (grey and black solid spectra, respectively). The dashed curve is the Gaussian QD distribution for $\Delta_{inh} = 8\ meV$ centered at the unrenormalized ground-state QD resonance. (b) Spontaneous emission linewidth versus inhomogeneous width. The dotted lines show $\Delta_{inh} = 10\ meV$, $15\ meV$ and $20\ meV$ correspond to $\Delta_{sp} = 24\ meV$, $36\ meV$ and $48\ meV$. At $\Delta_{inh} = 0$, the curve gives 5.4 meV for the room temperature, homogeneous (intrinsic) linewidth of an InAs QD.

Figure 1 illustrates the inhomogeneous broadening model, with the example of spontaneous emission. A laser sample has QD populations spreading over an energy range according to $n_{n,q}^{inh}$ (dashed curve, Fig. 1 (a)). Within the distribution, each group of QDs with similar transition energy emits a homogeneously-broadened spectrum (grey curve), which is calculated using Eqs. (1) - (4) and the Kubo-Martin-Schwinger transformation. [26] A luminescence measurement produces the inhomogeneously-broadened spectrum (solid black curve), which is computed by summing the different homogeneously-broadened spectra, each weighed by $n_{1,q}^{inh}$.

Since its measurement is relatively straightforward, the spontaneous-emission linewidth Δ_{sp} is often used to gauge QD inhomogeneity. A more direct measure of QD uniformity is the inhomogeneous width, Δ_{inh}, which gives the standard deviation in level energies. Figure 1(b) shows the Δ_{sp} to Δ_{inh} conversion, using the calculated homogeneously-broadened (intrinsic) spectrum. This paper considers active regions ranging from state-of-the-art to typical, with $10\ meV \leq \Delta_{inh} \leq 20\ meV$, corresponding to $24\ meV \leq \Delta_{sp} \leq 48\ meV$. [27] [28]

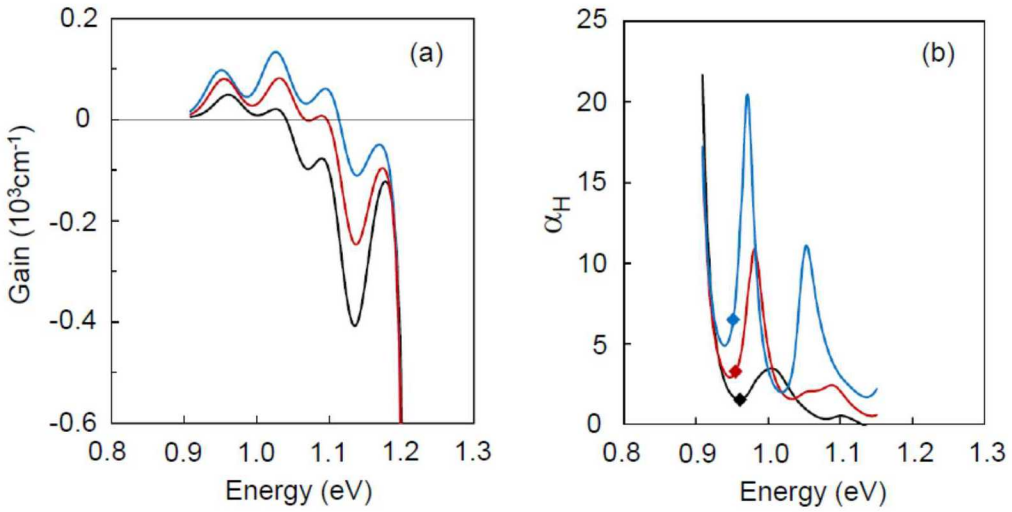

Figure 2. (a) Intensity gain and (b) linewidth enhancement factor spectra for undoped InAs QD structure with $20\ meV$ inhomogeneous width. The carrier densities are $3\times, 5\times, 7\times 10^{11}\ cm^{-2}$ (black, red and blue curves, respectively). In Fig. 1(b), the dots indicate the ground-state gain peak locations.

Figure 2 (a) shows the gain spectra for an undoped 7 nm $In_{0.15}Ga_{0.85}As$ QW with $5 \times 10^{10}\ cm^{-2}$ InAs QD density and $20\ meV$ inhomogeneous width. The resonances are from one ground-state and two excited-state transitions ($n = 1, 2\ and\ 3$, with degeneracies 1, 2 and 3, respectively). The absorption edge at 1.2 eV is from the GaAs QW exciton. Figure 2(b) shows the corresponding α_H spectra. The points indicate the ground-state gain peak values, which are all positive, with $\alpha_H(\nu_{pk}) \approx 2$ prior to onset of excited-state gain.

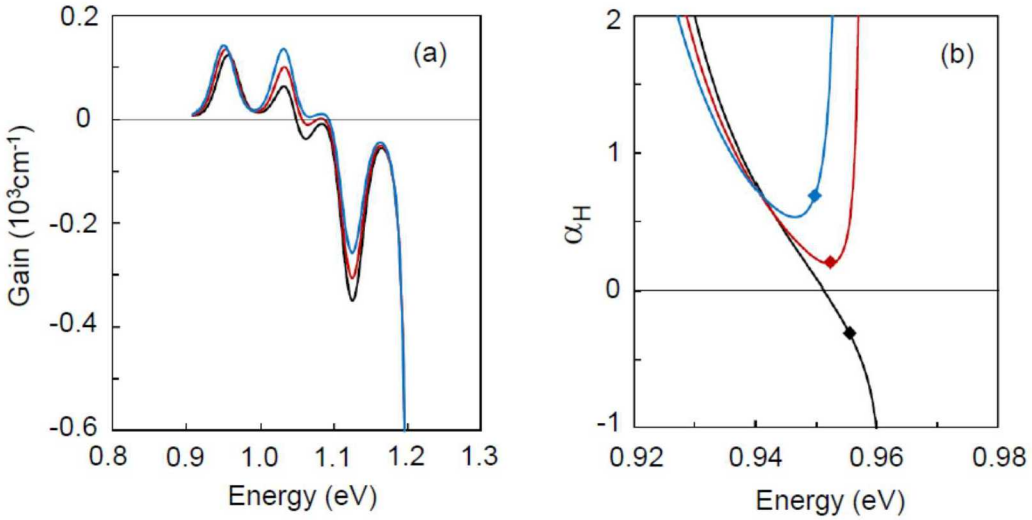

Figure 3. (a) Intensity gain and (b) linewidth enhancement factor spectra for InAs QD structure with $4 \times 10^{11}\ cm^{-2}$ p-dope density and $14\ meV$ inhomogeneous width. The carrier densities are $2.5 \times$, $3.0 \times$, $3.5 \times 10^{11}\ cm^{-2}$ (black, red and blue curves, respectively). In Fig. 3 (b), the dots indicate the gain peak locations and only the ground-state transition is plotted.

Figure 3(a) shows narrower and more distinct QD resonances when inhomogeneous broadening reduces to $14meV$, and with carrier densities are chosen to produce similar peak gains from the ground-state QD transition. The spectra show that the $4 \times 10^{11}\ cm^{-2}$ p-dope density leads to similar peak gains with lower carrier densities. Figure 3(b) depicts an interesting feature involving α_H at gain peak. The points indicate $\alpha_H(\nu_{pk})$ changing from negative to positive, suggesting that with proper laser design, $\alpha_H(\nu_{pk})$ can vanish.

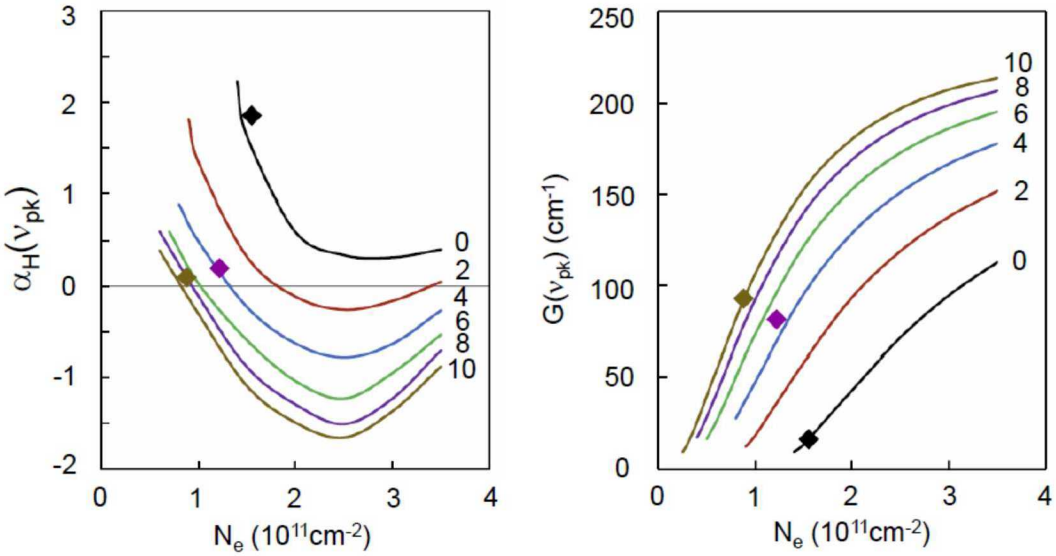

Figure 4. (a) Linewidth enhancement factor at gain peak and (b) peak gain per QD layer versus carrier density for ground-state transition and $10\,meV$ inhomogeneous broadening. The calculated curves labeled according to p-dope density in units of $10^{11}\ cm^{-2}$. The diamonds are from measurements for p-doped densities $N_p = 0,\ 5 \times 10^{11}\ cm^{-2}$ and $10^{12}\ cm^{-2}$ (black, blue-green and brown, respectively).

To further explore the vanishing of α_H, we repeated the calculations for broader ranges of carrier and p-dope densities. Figure 4 (a) shows that with sufficient p-dope density $\alpha_H(\nu_{pk}) = 0$ exists at specific carrier densities. Even for curves not crossing $\alpha_H(\nu_{pk}) = 0$, a minimum $\alpha_H(\nu_{pk})$ exists. Assuming laser operation with the saturated gain clamped at the threshold value, the desired carrier density may be achieved by cavity design via

$$G_{th} = G(\nu_{pk}) = \frac{1}{\Gamma L}[\alpha_{abs} - \ln(R_1 R_2)]\,, \tag{6}$$

where Γ is the confinement factor involving the waveguide and the QW embedding the QDs, L is the cavity length, α_{abs} is the intracavity absorption, R_1 and R_2 are the facet reflectivities. Figure 4 (b) shows plots of the calculated carrier density dependence of peak gain for the different p-dope densities.

Table 1. Experimental device parameters. Columns 1 to 3 are measured, column 4 is converted from column 2 using the growth sheet, columns 5 and 6 are from theory and experiment fits.

N_p ($10^{11}cm^{-2}$)	G_{mode} (cm^{-1})	α_H	G_{mat} (cm^{-1}/QD layer)	Δ_{inh} (meV)	N_e ($10^{11}cm^{-2}$)
0	10	1.855	16	10	1.63
5	50	0.198	81	10	1.20
10	57	0.097	93	10	0.88

To verify the calculations, we fabricated three laser batches with undoped, $5 \times 10^{11}\ cm^{-2}$ and $10^{12}\ cm^{-2}$ p-doped active regions. Each laser is epitaxially grown on Si substrate, with 1.25 mm long, uncoated-facet, Fabry-Perot cavity and 3.5 μm wide ridge. The active region has 5 QD layers, where each layer is as in the calculations. The mode-sum method [29] is used to obtain $\alpha_H(\nu_{pk})$ from amplified spontaneous emission spectra measured at different pulsed currents. The current pulse duration is 500ns, giving a 1% duty cycle. Figure 1 (b) is used to extract Δ_{inh} from measured spontaneous emission spectra. [30] [14] The material gain is that from a 7 nm $In_{0.15}Ga_{0.85}As$ QW embedded with a density of $5 \times 10^{10}\ cm^{-2}$ InAs QDs. Total gain region thickness is $5 \times 7nm$, inside a $285\ nm$ thick GaAs waveguide. [27] Table 1 lists the device parameters for one laser in each batch.

The experimental results are plotted as diamonds in Fig. 4. First, we used Fig.4 (b) to connect the experimental material gain to carrier density. Then, we plot in Fig. 4 (a), the measured $\alpha_H(\nu_{pk})$ versus the obtained carrier densities. The closeness of the experimental points to the respective theoretical curves indicates good theory and experiment agreement.

Figure 4 also indicates $\alpha_H(\nu_{pk}) < 0$, as observed in QD laser experiments in the form of absence of filamentation. [31] While eliminating filamentation is useful for high-power single-mode performance, [32] we chose instead to concentrate on datacom and telecom applications,

where there are more opportunities for QD lasers to contribute. There, the concerns are linewidth, chirp and feedback sensitivity, so that minimizing the absolute value of the gain-peak linewidth enhancement factor, $|\alpha_H(\nu_{pk})|_{min}$ is more important.

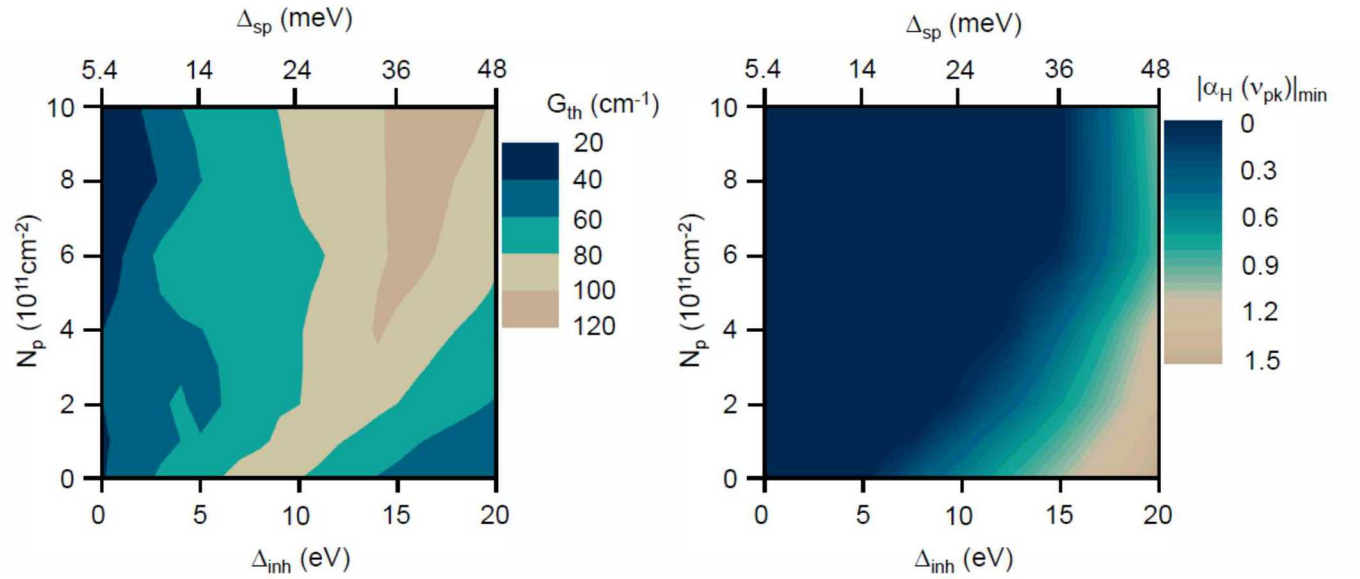

Figure 5. (a) Combinations of inhomogeneous width, p-dope density and threshold gain for lasing at gain peak with minimum absolute value of α_H. (b) Minimum absolute value of α_H at gain peak resulting from operating with combinations in Fig. 5(a).

Further parametric study suggests that lasing at $|\alpha_H(\nu_{pk})|_{min}$ depends on having certain combinations of Δ_{inh}, N_p and G_{th}. Figure 5 summarizes the results, with Fig. 5(a) giving the necessary combinations and Fig. 5(b) showing the resulting $|\alpha_H(\nu_{pk})|_{min}$ with those combinations. Only ground-state lasing is presented, because most experimental efforts for improving performance are concentrated there.

Of interest is the subset of Δ_{inh}, N_p and G_{th} giving $\alpha_H(\nu_{pk}) = 0$. Figure 5(b) indicates a sizable region, reachable with present QD lasers. Within this region, QD non-uniformity may be compensated by p-doping. For $\Delta_{inh} < 8\,meV$ ($\Delta_{sp} < 20\,meV$), p-doping is even unnecessary. When $\Delta_{inh} > 16\,meV$ ($\Delta_{sp} > 38\,meV$), $\alpha_H(\nu_{pk}) = 0$ is unachievable regardless of p-dope

density. The challenge is fabricating a resonator accurately for a prescribed G_{th}. Fortunately, there are combinations that are less sensitive to G_{th}, e.g., with $\Delta_{inh} \approx 10\ meV$, which is state-of-the-art QD uniformity [27] and $N_p > 2 \times 10^{11}\ cm^{-2}$, Fig. 5(a) indicates a wide range of $80 cm^{-1} < G_{th} < 100\ cm^{-1}$. For an active region consisting of 6 QD layers in a 0.3 μm thick, 0.4 mm long waveguide with uncoated facets, Eq. (6) gives $G_{th} = 96 cm^{-1}$, assuming $\alpha_{abs} = 3\ cm^{-1}$. For $1.3 \mu m$ lasing wavelength, this translate to a resonator Q factor of 3100. Not shown in the plots, but relevant to modulation bandwidth and threshold current are differential gain and threshold carrier density ranges of $2 \times 10^{-16}\ cm^2 < dG/dN_e^{3D} < 4.3 \times 10^{-16}\ cm^2$ and $1.5 \times 10^{11} cm^{-2} < N_e < 2.8 \times 10^{11}\ cm^{-2}$, for lasing with $\alpha_H(\nu_{pk}) = 0$. At the low N_e limit, the threshold current density is $J_{th} \sim 320\ A/cm^2$, using $J_{th} = eN_e\eta^{-1}\{J_{sp} + N_e[A + C(N_e^{3D})^2]\}$, where $J_{sp} = 3.4\ A/cm^2$ is from the gain calculation. Also, we use defect (Shockley-Read-Hall) loss $A = 1.2 \times 10^9\ s^{-1}$, injection efficiency $\eta = 0.6$ and Auger coefficient $C = 10^{-28}\ cm^6\ s^{-1}$, either reported in the literature or extracted from characterizing our QD active regions. [30] [33]

In summary, QD lasers may be configured to operate with linewidth enhancement factor $\alpha_H = 0$. The beneficial effects are reduced linewidth, chirp elimination and reduced optical feedback sensitivity. That $\alpha_H = 0$ can occur at the gain peak simplifies device design and minimizes power consumption, which are important considerations in datacom and telecom applications. Many-body renormalizations and dephasing significantly contributed to QD α_H. The parametric study, supported with experiment, provides the necessary combinations of inhomogeneous linewidth, p-dope density and threshold gain, that are reachable by present QD lasers.

This research was supported by Advanced Research Projects Agency-Energy (ARPA-E) No. DE-AR000067, the U.S. Department of Energy under Contract No. DEAC04-94AL85000, the U. S. Army Space and Missile Defense Command (USASMDC) under Contract 214971, and to the Directed

Energy Joint Transition Office (DE-JTO) under Project 17-S&A-0586. This work was performed, in part, at the Center for Integrated Nanotechnologies, an Office of Science User Facility operated for the U.S. Department of Energy (DOE) Office of Science. Sandia National Laboratories is a multimission laboratory managed and operated by National Technology & Engineering Solutions of Sandia, LLC, a wholly owned subsidiary of Honeywell International, Inc., for the U.S. DOE's National Nuclear Security Administration under contract DE-NA-0003525. The views expressed in the article do not necessarily represent the views of the U.S. DOE or the United States Government.

[1] Y. Arakawa and H. Sakaki, "Multidimensional quantum well laser and termperature dependence of its threshold current," *Appl. Phys. Lett.,* vol. 40, pp. 939-941, 1982.

[2] N. Kirstaedter and et al., "Low threshold, large T0 injection laser emission from (InGa)As quantum dots," *Electron. Lett.,* vol. 30, pp. 1416-1417, 1994.

[3] R. Mirin, A. Gossard and J. Bowers, "Room temperature lasing from InGaAs quantum dots," *Electron. Lett.,* vol. 32, p. 1732, 1996.

[4] D. Bimberg and U. W. Pohl, "Quantum dots: Promises and accomplishments," *Mater Today,* vol. 14, pp. 388-397, 2011.

[5] T. Kageyama and et al., "Extremely high termperature (220C)continuous-wave operation of 1300-nm-range quantum-dot lasers," *Proc. Conf. Lasers Electro-Opt. Eur. 12 Eur. Quantum. Electron. Conf. (CLEO EUROPE/EQEC),* p. 1, May 2011.

[6] A. Y. Liu, S. Srinivasan, J. Norman, A. C. Gossard and J. E. Bowers, "Quantum dot lasers for silicon photonics," *Photon. Res.,* vol. 3, pp. B1-B9, 2015.

[7] J. Duan, H. Huang, B. Dong, D. Jung, J. C. Norman, J. E. Bowers and F. Grillot, "1.3-um reflection insensitive InAs/GaAs quantum dot lasers directly grown on silicon," *IEEE Photonics Tech. Lett.,* vol. 31, pp. 345-348, 2019.

[8] M. W. Fleming and A. Mooradian, "Fundamental line broadening of single-mode (GaAs)As diode lasers," *Appl. Phys. Lett.,* vol. 38, pp. 511-513, 1981.

[9] T. L. Koch and J. E. Bowers, "Narure of wavelength chirping in directly modulated semiconductor lasers," *Electron. Lett.,* vol. 20, pp. 1038-1039, 1984.

[10] R. Tucker, "High-speed modulation of semiconductor lasers," *IEEE Trans. Electron Devices,* Vols. ED-32, pp. 2572-2584, 1985.

[11] R. Tkach and A. Chraplyvy, "Regimes of feedback effects in 1.5um distributed feedback laers," *J. Lightw. Technol.,* Vols. LT-4, pp. 1655-1661, 1986.

[12] C. Henry, "Theory of linewidth of semiconductor lasers," *IEEE J. Quantum Electron.,* Vols. QE-18, pp. 259-264, 1982.

[13] H. Vahala and A. Yariv, "Semiclassical theory of noise in semiconductor lasers -- Part II," *IEEE J. Quantum Electron.,* Vols. QE-19, pp. 1102-1109, 1983.

[14] Z. Zhang, D. Jung, J. C. Norman, P. Patel, W. W. Chow and J. E. Bowers, "Effects of modulation p doping in InAs quantum dot lasers on silicon," *Appl. Phys. Lett.,* vol. 113, pp. 061105-4, 2018.

[15] Z. Zhang, D. Jung, J. C. Norman, W. W. Chow and J. E. Bowers, "Linewidth enhancement factor in InAs/GaAs quantum dot lasers and its implication in isolator-free and narrow linewidth applications," *IEEE J. Selected Topics in Quantum Electron.,* vol. 25, p. 1900509, 2019.

[16] M. V. Maximov and et al., *Phys. Rev. B,* vol. 62, pp. 16671-16680, 2000.

[17] H. Y. Liu and et al., *Journ. Appl. Phys.,* vol. 93, pp. 2931-2936, 2003.

[18] J. Duan, D. Jung, Z. Zhang, J. Norman, J. E. Bowers and F. Grillot, "Semiconductor quantum dot lasers epitaxially growth on silicon with low linewidth enhancement factor," *Appl. Phys. Lett.,* vol. 112, p. 251111, 2018.

[19] H. C. Schneider, W. W. Chow and S. W. Koch, "Many-body effects in the gain spectra of highly excited quantum dot lasers," *Phys. Rev. B,* vol. 64, p. 115315, 2001.

[20] M. Lorke, F. Jahnke and W. W. Chow, "Excitation dependences of gain and carrier-induced refractive index change in quantum-dot lasers," *Appl. Phys. Lett.,* vol. 90, pp. 051112-051114, 2007.

[21] R. Lang and K. Kobayashi, "External optical feedback effects on semiconductor injection laser properties," *IEEE J. Quantum Electron.,* vol. 16, pp. 347-355, 1980.

[22] L. A. Coldren, S. W. Corzine and M. L. Masanovic, Diode lasers and photonic integrated circuits, Hoboken: John Wiley & Sons, 2012.

[23] H. C. Schneider, W. W. Chow and S. W. Koch, "Excitation-induced dephasing in semiconductor quantum dots," *Phys. Rev. B,* vol. 70, pp. 235308-1-235308-4, 2004.

[24] J. Seebeck, T. R. Nielsen, P. Gartner and F. Jahnke, "Polarons in semiconductor quantum dotsand their role in the quantum kinetics of carrier relaxation," *Phys. Rev. B,* vol. 71, pp. 125327-1-125327-6, 2005.

[25] H. C. Scbneider, S. W. Koch and W. W. Chow, "Anomalous carrier-induced dispersion in quantum-dot active media," *Phys. Rev. B,* vol. 66, p. 41310(R), 2002.

[26] C. H. Henry, R. A. Logan and F. R. Merritt, "Measurement of gain and absorption spectra in AlGaAs buried heterostructure lasers," *J. Applied Physics,* vol. 51, pp. 3042-3051, 1980.

[27] J. C. Norman, D. Jung, Z. Zhang, Y. Wan, S. T. Liu, R. W. Herrick, W. W. Chow, A. C. Gossard and J. E. Bowers, "A review of high-performance quantum dot lasers on Silicon," *IEEE J. Quantum Electron.,* vol. 55, p. 2000511, 2019.

[28] T. Septon and et al., "Large linewidth reduction in semiconductor lasers based on atom-like gain material," *Optica,* vol. 6, pp. 1071-1077, 2019.

[29] D. T. Cassidy, "Technique for measurement of gain spectra of semiconductor diode lasers," *J. Appl. Phys.,* vol. 56, pp. 3096-3099, 1984.

[30] W. W. Chow, A. Y. Liu, A. C. Gossard and J. E. Bowers, "Extraction of inhomogeneous broadening and nonradiative losses in InAs quantum-dot lasers," *Appl. Phys. Lett.,* vol. 107, p. 1171106, 2015.

[31] P. M. Smowton, E. J. Pearce, H. C. Schneider and W. W. Chow, "Filamentation and linewidth enhancement factror in InGaAs quantum dot lasers," *Appl. Phys. Lett.,* vol. 81, pp. 3251-3253, 2002.

[32] P. Kirkby, A. Goodwin, G. Thompson and P. Selway, "Observation of self-focussing in sripe geometry semiconductor laser and the development of a comprehensive model of their operation," *IEEE J. Quantum Electron.,* Vols. QE-13, pp. 705-719, 1977.

[33] I. P. Marko, A. D. Andreev, A. R. Adams, R. Krebs, J. P. Reithmaier and A. Forchel, "The role of Auger recombination in InAs 1.3-um quantum-dot lasers investigated using high hydorstatic pressure," *IEEE J. Selected Topics in Quantum Electron.,* vol. 9, pp. 1300-1307, 2003.

[34] W. W. Chow and F. Jahnke, "On the physics of semiconductor quantum dots for applications in lasers and quantum optics," *Progr. Quantum Electron.,* vol. 37, pp. 109-184, 2013.